Saturated x-ray lasers at 196 and 73 Å pumped by a picosecond traveling-wave excitation

R. E. King,[1] G. J. Pert,[1] S. P. McCabe,[1] P. A. Simms,[1] A. G. MacPhee,[2] C. L. S. Lewis,[2] R. Keenan,[2] R. M. N. O'Rourke,[2] G. J. Tallents,[1] S. J. Pestehe,[1] F. Strati,[1] D. Neely,[3] and R. Allott[3]

[1]*Department of Physics, The University of York, Heslington, York YO10 5DD, United Kingdom*

[2]*School of Mathematics and Physics, Queen's University of Belfast, Belfast BT7 1NN, United Kingdom*

[3]*The Rutherford Appleton Laboratory, Chilton, Didcot, OXON OX11 0QX, United Kingdom*

(Received 13 March 2001; published 12 October 2001)

Traveling-wave irradiation with a laser pulse of duration ~1 picosecond has been shown to achieve saturated operation of Ne- and Ni-like x-ray lasers. Gain at 196 Å was confirmed by observation of both forward and backward x-ray laser beams from a germanium plasma under ideal and nonideal traveling-wave conditions at a small signal gain of >40 cm^{-1}. Saturation was observed for targets >4 mm long consistent with a model of laser amplification along the plasma medium and with the output of a detailed ray-tracing post-processor coupled to a hydrodynamic and atomic physics code. Ni-like samarium targets, pumped under ideal traveling-wave conditions exhibited a small signal gain of ~19 cm^{-1} at 73 Å with saturation observed for targets 8 mm long.

DOI: 10.1103/PhysRevA.64.053810 PACS number(s): 42.55.Vc, 32.30.Rj, 42.60.By, 52.50.Jm

I. INTRODUCTION

The efficiency of pumping soft x-ray lasers (XRLs) based on a laser-produced plasma medium has increased by more than three orders of magnitude in the last decade [1–6]. Scaling to shorter wavelength operation has been achieved through the use of higher Z targets allowing the efficient operation of nickellike, as well as neonlike x-ray lasers. Saturated lasing at wavelengths as short as 5.9 nm has been observed [7,8]. Two developments have led to the enhancement of efficiency. First, performing plasmas using a prepulse incident before the main pumping pulse has reduced refraction, enhanced the volume of gain region [9] and increased the absorption of the laser pump [10]. Second, the development of chirped pulse amplification (CPA) has enabled small and moderately sized lasers to produce high-focused irradiances in short duration pulses. Such pulses efficiently pump x-ray laser gain as over ionization to the next higher ionization stage (F-like or Co-like) is reduced [11,12]. Gain in neonlike ions with short-pulse (~psec) pumping was first observed at the Max Born Institute in Berlin [13] and the first observations of lasing from nickellike ions (Sn and Sm) were made at the Rutherford Appleton Laboratory (RAL) using a traveling wave pump [14], at Lawrence Livermore National Laboratory (LLNL) [15] and at Laboratoire pour l'Utilisation des Lasers Intense (LULI) [16,17]. Here, we report application of a traveling wave-pumping technique that enables us to achieve saturated x-ray laser output at the shortest wavelength to date using ~psec pulse irradiation.

Collision-pumped soft x-ray lasers have traditionally used optical lasers with pulses of duration 0.1–1.0 nsec in a line focus at 10^{13}–10^{14} Wcm^{-2} to produce and ionize plasma from a suitable solid target. Intrinsic to the heating process was a requirement to simultaneously generate both the hydrodynamic structure and the population inversion on specific transitions. This required a balance between collisional (monopole) excitation and fast radiative decays. On the long (subnanosecond) timescales required to allow the plasma hydrodynamics to evolve, this approach leads to a pumping regime with the upper-laser level state populations having time to approach thermal equilibrium with each other and with adjacent higher levels through collisions. Increasing the plasma temperature, by using higher irradiance, to increase collision pump rates, and hence, inversion density eventually fails as the plasma over ionizes and the fractional abundance of the lasant ion becomes too low to sustain a useful gain coefficient.

Short-pulse pumping decouples the two main phases in generating inversion and gain [18]. A long pulse is used to produce and ionize a plasma of the desired ionic composition, as before, but it does not have to heat the plasma to high temperature. Ideally, the temperature reached should be just sufficient to produce a large fractional abundance in the ground state of the neonlike or nickellike ionization stage, but too low to cause significant excitation of the upper-laser levels. The plasma is allowed to expand hydrodynamically to a point where the correct ion stage is located in a region of optimum electron density (usually in the range $(1-6)\times10^{20}$ cm^{-3}) and small density gradient. At this time, the population inversion is pumped by injecting an ultra-short pulse of picosecond duration at high irradiance (e.g., up to 2×10^{15} Wcm^{-2}) into the preprepared plasma. This raises the electron temperature very rapidly to values in excess of a kilovolt and leads to transient collisional excitation and large values of gain coefficient. Typical simulations for both Ne-like and Ni-like ions indicate gain coefficients in excess of 100 cm^{-1} can be achieved on picosecond timescales before further ionization reduces the gain [19]. The penalty paid in this scheme is that the consequent short-lived gain duration T_G, demands that the amplifier length cannot be longer than about cT_G, unless a traveling wave pump is used to keep the excitation in phase with the amplifying group of photons. The advantage of the short-pulse pumping is that saturation of output may be achieved with relatively short (several mm) amplifier lengths. This leads to bright x-ray laser output with picosecond duration pulses and a pump-energy requirement that is modest in terms of both the nanosecond and picosecond drive pulses.

Saturated output from x-ray lasers pumped with short ~psec pulses has been reported for Ni-like Sn [20] and Ni-like Mo, Pd, Ag, Cd, and Sn [21] at wavelengths down to 120 Å. In this paper, we report the demonstration and mod-

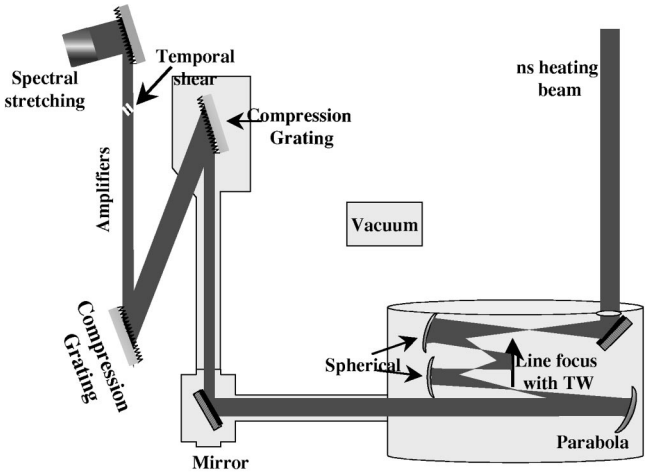

FIG. 1. Experimental setup for TW CPA experiments using the Vulcan laser at RAL. The long-pulse (preplasma formation) and short-pulse (transient inversion pump) beams are line focused using off-axis spherical mirrors and the relative arrival time of the psec and nsec beams can be varied. The line-focus TW arrow points towards the North spectrometer, which receives the brightest XRL signal.

eling of traveling-wave operation of both Ne-like and Ni-like x-ray lasers with saturated outputs at wavelengths as short as 73 Å. The picosecond-pump pulse with energy up to ~ 50 J is generated in the VULCAN laser amplifier chain using chirped pulse amplification (CPA) technology [22].

II. EXPERIMENTAL ARRANGEMENT

Guided by simulations, the basic pumping scheme used three 1.06 μm laser pulses. For Ne-like Ge, the most effective pumping scheme investigated used three pulses. Two 280 psec full width at half maximum (FWHM) Gaussian pulses with average irradiance $\sim 10^{12}$ Wcm^{-2} (first pulse) and $\sim 10^{13}$ (second pulse) and separated by 2 nsec were used to prepare the preformed plasma. The third pulse was <3 psec FWHM, at irradiance $\sim 10^{15}$ Wcm^{-2} and arrived to interact with the preformed plasma during the trailing edge of the second pulse. In contrast, we found that the traveling wave-pumped Ni-like Sm x-ray laser was improved by using a single 280 psec heating beam and a single-short pulse beam. All three pulses were derived from the same yttrium-lithium-fluoride (YLF) oscillator. The CPA pulse was stretched, amplified, and then compressed prior to entering the target chamber. The 280 psec heating pulses were split from the CPA line after stretching, diverted to an alternative amplifier chain and then directed into the target area. This mode of operation eliminated jitter in the arrival time of the three laser pulses on target.

Each pulse was focused to a common line focus of ~ 100 μm width and ~ 12 mm length. A tilted spherical mirror imaged a spot focus of each beam created by an off-axis parabolic mirror to the line focus (Fig. 1). Targets were made from either germanium or samarium evaporated on to polished glass substrates with length ranging from 1 mm up to 10 mm. The targets were centered in the line focus with the target normal horizontal.

To achieve pumping with the picosecond pulse in an excitation wave traveling at the speed of light c it is necessary to tilt the wave front of this beam so that it intercepts the target plane at 45° [23–26]. The method adopted at RAL for traveling-wave (TW) pumping combines the intrinsic tilt in the wave front inherent to the off-axis focusing optics used with an additional component introduced using a diffraction grating, as shown in Fig. 1 [22]. The grating was situated downstream of the pulse chirping system, which was located at an early stage in the laser amplifier chain. As a result, it was necessary to take into account the change in beam diameter and hence wave-front tilt angle as the pulse propagated through the main optical amplifier chain. Without the diffraction grating, the intrinsic traveling-wave speed was $2.9c$ and we henceforth refer to this condition as the nontraveling-wave (NTW) mode.

The total path length for the CPA pump beam depended on whether or not the traveling wave was used, as the additional grating introduced an optical delay. For optimum tuning of the CPA pulse compression, the pulse stretcher gratings were adjusted to compensate for the change in dispersion introduced by the traveling-wave grating. This introduced a change in path length common to all three pumping beams, so that the relative timing was not affected. The CPA pulse length, the speed of the traveling wave, and the relative timing of the long and short pulses were set and verified at the target plane using a Hamamatsu *S*1 optical streak camera with ~ 300 fsec resolution. For full energy shots on target, the optical streak camera could not be used and the CPA pulse length was measured using a third-order autocorrelator cross calibrated against the fast optical streak camera. The relative timing of the CPA pulse and the long pulses was monitored on a shot-to-shot basis using kilovolt x-ray streak records. Relative beam timing was adjusted with a mirror slide trombone in the long-pulse beam line. For the Ge target shots, the pulse length without traveling wave was measured to be 1.0 ± 0.2 psec using an autocorrelator. The pulse was stretched to 2.7 ± 0.2 psec when the traveling wave was introduced. For the Sm target shots, the pulse length was 0.8 ± 0.2 psec without traveling wave and 1.0 ± 0.2 psec with the traveling wave. The difference in pulse length between the two sets of measurements was due to different degrees of optimization of the pulse stretcher.

To measure the soft x-ray signal from the plasma, two grazing incidence, flat-field spectrometers were used. Each comprised a variable pitch (mean groove density ~ 1200 mm^{-1}), a concave gold grating of 5 m radius, and a 16-bit, back-thinned charge-coupled device (CCD) system [27]. The spectrometers were mounted axially to observe the x-ray laser signals emitted in both the preferred, traveling-wave direction (north) and in the opposite direction (south). The spectrometers sampled the XRL beams with angular acceptance widths, $\Delta\theta_{\mathrm{H}}$ and $\Delta\theta_{\mathrm{V}}$, in the horizontal and vertical planes, where the horizontal plane is defined by the target normal and the TW pumping direction and the vertical plane is parallel to the target surface. In these experiments $\Delta\theta_{\mathrm{H}}$ ~ 40 mrad and ~ 28 mrad, and $\Delta\theta_{\mathrm{V}} \sim 7$ mrad and ~ 5 mrad

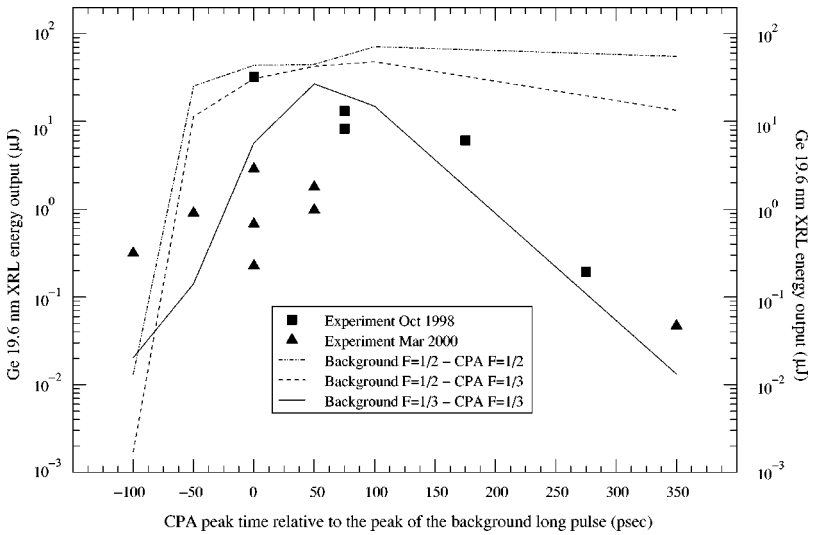

FIG. 2. X-ray laser output dependence on the arrival time of the short CPA pulse relative to the peak of the long pulse for 5mm Ge targets. Results from two sets of experiments are shown with different symbols. Simulations with different values of the fraction of laser energy available for absorption F are shown as curves.

for the North and South spectrometers respectively. Although horizontal angular profiles are effectively measured directly (see Figure 6 later) the vertical intensity distribution is not. For the purposes of estimating the total XRL beam energy in each direction by integration over solid angle, we assume the vertical beam divergence is twice the measured horizontal value and that we sample on the peak of a Gaussianlike distribution; this is broadly consistent with previous near and far-field measurements of non-CPA pumped cases, and also with simulated far-field patterns obtained using the code RAYTRACE discussed later. We estimate that this approach, coupled with other uncertainties such as grating efficiency, filter transmissions and quantum efficiency of the CCD's, leads to an overall factor of <2 uncertainty in the south-beam energy measurements, with the north-beam estimates more reliable and probably accurate to better than 50%.

Uniformity of the pump-laser heating along the target was monitored by two space-resolving Bragg crystal spectrometers. One observed the plasma from $\sim 45°$ above and the other observed the plasma in the horizontal plane. The dispersion elements were convex potassium acid phthalate (KAP) crystals with 300 mm radius of curvature and the time-integrating detectors for both of the spectrometers were 16-bit CCD's [27]. The spectral range for both spectrometers was set to cover ~ 7–10 Å to record the resonance line emission from the Ne- and F-like Ge and Ni- and Co-like Sm ions. A third spectrometer with similar spectral range was also mounted with line of sight $\sim 45°$ above the horizontal to obtain time-resolved spectral information. The detector in this was a Kentech x-ray streak camera with ~ 10 psec temporal resolution of emissions from a ~ 1 mm space-integrated length near the center of the target. A differentially magnifying crossed-slits camera, filtered to detect emissions at >1 keV, was used with a time-integrating 16-bit CCD to monitor the line-focus width as a function of distance along the target. The system achieved ~ 10 μm resolution across the target and ~ 100 μm resolution along the target. All these diagnostics provide useful data for detailed comparisons with simulations but, for now, we simply note that they ensured good reproducibility of experimental conditions for the lasing signal data reported here.

III. EXPERIMENTAL RESULTS

All observed x-ray lasing action was initiated by the CPA pulse. This was confirmed by noting that in the absence of the CPA pulse, the preplasma alone could not generate enough gain to produce a detectable output at the lasing wavelength.

A. Germanium Ne-like laser

A sequence of shots on 5 mm long Ge targets was taken to determine the optimum delay between the main long pulse and the short pulse with the traveling wave switched on (Fig. 2). The experiment was subsequently repeated with similar results [28], which have also been included in this plot. A relatively short target length was chosen to optimize the sensitivity of the measurement by avoiding both very small and very saturated signal strengths. The short-pulse irradiance was $\sim 1.5\times 10^{15}$ Wcm^{-2}, the main long-pulse irradiance was $\sim 5\times 10^{12}$ Wcm^{-2}, and a 10% prepulse arrived 2 nsec early. The optimum x-ray laser output from both experiment and simulation (discussed below) is when the short-laser pulse is incident approximately 50 psec after the peak of the long pulse. These results also show the shot-to-shot reproducibility of the experiment, and hence, give an indication of the sensitivity of pulse buildup to shot-to-shot variations in the exact irradiance and target conditions as the variance is much larger than the precision of the energy measurement.

The gain coefficient for the system was measured with a sequence of shots taken with target length ranging from 2–9 mm as shown in Fig. 3. The long- and short-pulse separation for this length scan was 80 psec. To examine the effect of the traveling wave, a further sequence of shots was taken with target length ranging from 2–9 mm but with the traveling wave switched off. The error bars in Fig. 3, and elsewhere, reflect the shot-to-shot variation where more than one measurement was made.

The two data sets in Fig. 3 represent the x-ray laser output measured under TW and NTW conditions. The signal growth curves are similar for short target lengths, but diverge for lengths $\geqslant 3.5$ mm. Since the x-ray transit time along a 3.5 mm target is ~ 10 psec we infer that this gives the charac-

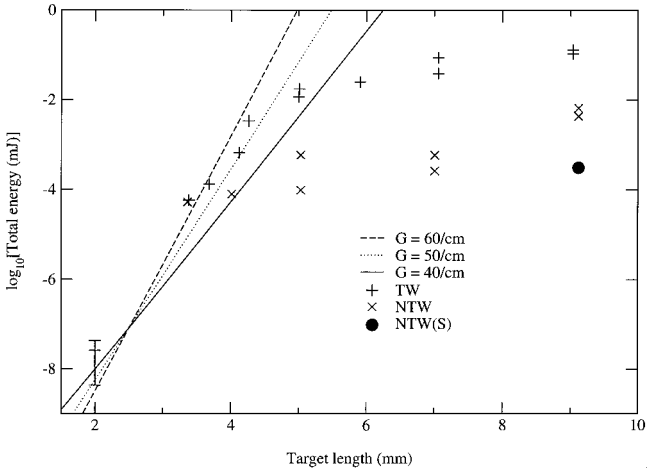

FIG. 3. Experimental data showing growth curve for 196 Å Ge signal with SSG >40 cm^{-1} leading to strongly saturated output of ~ 0.1 mJ when pumped with TW ($V=c$). For NTW ($V=2.9c$), outputs at each end of target (N and S) are consistent with a pulse duration of ~ 10 psec.

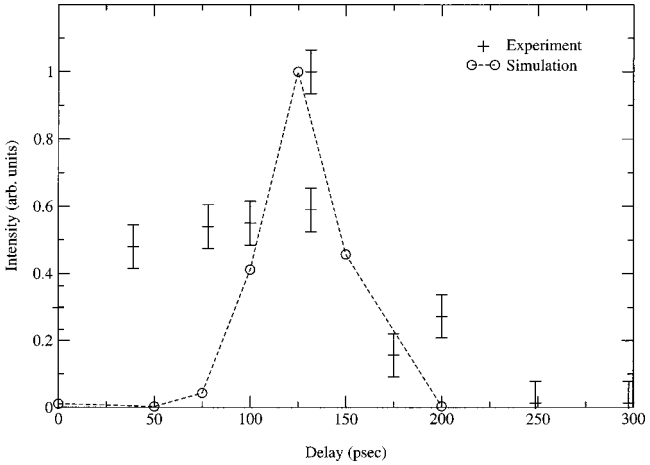

FIG. 4. XRL output dependence on arrival time of short CPA pulse relative to peak of long pulse for 9 mm Sm (73 Å) targets.

teristic order of magnitude of the gain duration in the system and that it provides an estimate of the XRL pulse length. Figure 3 also shows analytic growth curves based on the Linford formula [29] for a range of small signal gain coefficients, indicating that the peak gain coefficient achieved is >40 cm^{-1}. The total output energy from the 9 mm target was $\sim 100\mu$J. An estimate of the saturation irradiance is derived from Figure 3, using a fourth order polynomial fit to the TW data to locate the point where the small signal gain (SSG) coefficient is reduced to half its peak value. The saturation irradiance is reached with a target length of ~ 4.5 mm, and has a value of $\sim 2\times 10^{10}$ Wcm^{-2}. These values are in close agreement with simulation, where the ray averaged values for the gain coefficient and saturation irradiance at the time of maximum output are 50 cm^{-1} and 1.6×10^{10} Wcm^{-2}, respectively. Assuming a 10 psec x-ray laser-pulse length and estimating an exit aperture of dimensions 25 μm horizontal and 55 μm vertical, the exit irradiance at 9 mm corresponds to an irradiance in the plasma of $\sim 7\times 10^{11}$ Wcm^{-2}, which is well into the saturated regime [30].

Measurements made on the flat-field spectrometer in the south (counter-propagating direction) with the traveling wave switched off (NTW) showed negligible output of the x-ray laser line, as would be expected for a short duration gain period, predicted to be ~ 30 psec. The south (S) spectrometer is less sensitive than the north (N) spectrometer, partly due to being located farther from the target to avoid the short-pulse beam. The only measurable signal in the south direction when the TW was switched off was from a 9 mm target; this is the data point marked NTW(S) in Fig. 3.

B. Samarium Ni-like laser

Having established the effectiveness of the TW pump, we shot samarium-coated targets with the same experimental arrangement, but at $\sim 2\times$ higher pump irradiance. Although initially guided by modeling that also used a prepulse we found that, for Sm, a 10% prepulse on the long-pulse beamline damaged the conditions for gain at 73 Å, typically reducing the potential output by a factor of ~ 3. Our data for the traveling-wave pumped Ni-like Sm x-ray laser was produced using a single 280 psec heating beam and a single short-pulse beam. The arrival time of the CPA pulse relative to the peak of the long pulse was optimized as shown in Fig. 4, by taking a sequence of shots with different delays on the long-pulse beam line. The optimum pulse separation was found to be ~ 130 psec. A further sequence of shots was taken to measure the gain coefficient at the optimum pulse separation as shown in Fig. 5. A gain coefficient of ~ 19 cm^{-1} was measured for this transition. The maximum integrated x-ray laser output energy for the 73 Å Sm laser was ~ 1.5 μJ and based on modeling parameters, this corresponds to an output irradiance of $\sim 10^{10}$ Wcm^{-2}. For comparison, the ray-averaged parameters for the gain coefficient and saturation irradiance from simulation are 21.5 cm^{-1} and 3×10^{10} Wcm^{-2}, respectively. Saturation has been achieved

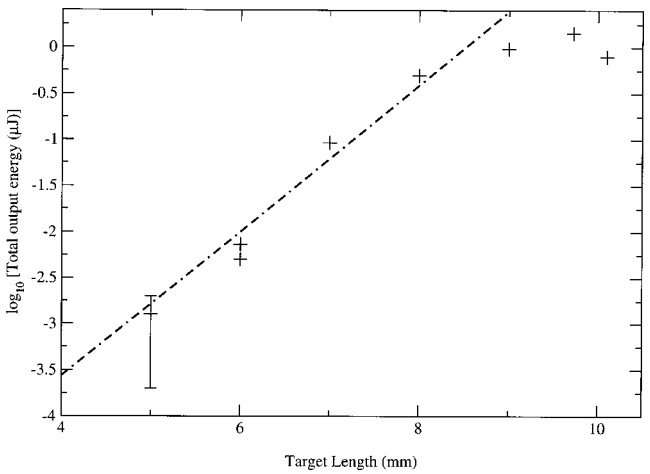

FIG. 5. Growth curve for Sm at 73 Å with small signal gain ~ 19 cm^{-1} shown by Linford fit. The gain-length product for >8 mm is >15, indicating a roll over into saturation with an output pulse energy of ~ 1.5 μJ at an estimated plasma exiting irradiance of $\sim 10^{10}$ Wcm^{-2}.

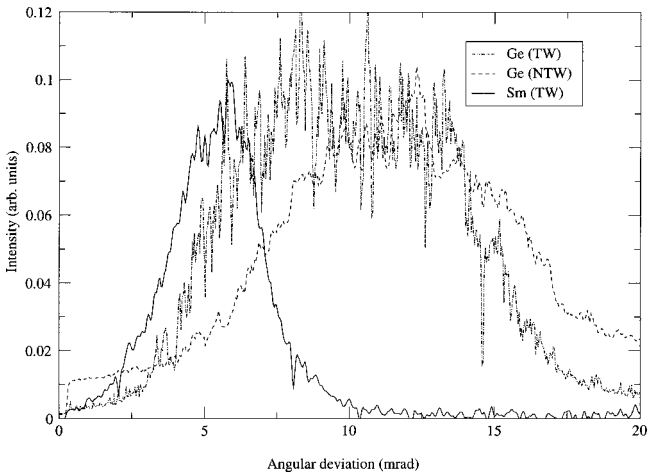

FIG. 6. Horizontal angular distributions for outputs from 9 mm targets of Ge TW (dotted) and NTW (dashed), and Sm (solid), indicating a relatively less refracted beam in the Sm case.

with the longest Sm targets, but the rolling over of the signal at approximately 9 mm is compounded by the reducing short-pulse irradiance at the end of the target, as the target length is similar to that of the line focus. No signals were detected from Sm targets on the backward flat-field spectrometer, again confirming the effectiveness of the matched traveling-wave pump.

Figure 6 shows typical angle-resolved line outs from the north flat-field spectrometer for 9 mm Ge and Sm targets. The beam divergence for Ge is ~ 10 mrad and the beam-pointing angle from the target axis is ~ 9 mrad. The angular profiles of the germanium laser recorded under TW and NTW conditions show that refraction condition must be similar in both TW and NTW pump conditions in agreement with simulation. Compared to the Ge data, the Sm laser has much-reduced divergence and pointing angle, measured at 2.8 and 4.9 mrad, respectively. This is expected, due to the reduced refraction effects at the shorter wavelength, and the narrower gain zone for this laser.

IV. MODELING OF EXPERIMENTAL RESULTS

The experimental data have been compared to outputs from numerical simulations for both germanium and samarium experiments. The numerical simulations derive from a three-dimensional (3D) ray-trace post-processing of the space-time output from the 1.5-D fluid and collisional-radiative atomic code EHYBRID [31]. The RAYTRACE code [5], which includes saturation effects, simulates the TW case by following the amplified spontaneous emission signals from a set of intervals through the gain pulse and time integrating the resultant outputs. The germanium calculations used a modified data set, which did not include the empirical adjustment to the $J=0$-$J=0$ monopole collisional-excitation rate, to the upper-laser state, applied earlier [31]. The samarium set was generated from the gadolinium data used in Ref. [12] adapted with values from GRASP [32] and Ref. [33]. The absolute energy values from the numerical model and from experimental measurements are derived independently and are in good agreement, particularly in the long target TW case.

An analytic model has also been used to aid the interpretation of the data. This has been developed from the standard model of steady-state amplified spontaneous emission (ASE) lasing, by modifying the unidirectional model, which considers the laser beam generated in each direction along the axis as independent, to include a time-varying gain and spontaneous emission rate [20,34,35]. The values of these parameters can be specified quite generally, or as in this case, from the output of detailed simulation. The applicability and accuracy of the model were examined in Ref. [35] by comparing values yielded by the model to a simulation of the germanium TW experiment. The model can be simply used to treat both TW and NTW wave systems with arbitrary line profiles. We have recently extended the model to treat the time-dependent bidirectional ASE configuration [36], where the saturation of the forward going laser radiation modifies the backward, and *vice versa*.

The model calculates the output from a laser rod of specified spontaneous emission and saturation irradiances, gain and area with prescribed time profiles. It is particularly useful for treating bidirectional output in the NTW case, which is difficult to simulate with the RAYTRACE code. As the NTW data is more scattered than the TW, we have tested the consistency of the model against the experiments, rather than an accurate simulation. In this paper we have assumed a homogeneous line profile when using the model, for the reasons discussed in Ref. [35]. In order to apply the model it is necessary to have appropriate average values for the input parameters. Since the density profile is nearly constant over the lasing time, the ray paths at different times are nearly identical. However, in the NTW case, only a limited length of the gain medium is effectively active. Suitable values of the necessary input parameters for the model are obtained from the corresponding values generated by RAYTRACE at the same output energy (i.e., gain-length product) in the TW case, which are in good agreement with the gain and saturation irradiance measured experimentally. Although the model is quite sensitive to the input values, most of these are slowly varying throughout the pulse. However, the ray-averaged spontaneous irradiation (which is assumed constant in the model) does have significant variation both in time and over different scale lengths, thereby introducing uncertainty into the final model results.

The EHYBRID code using 100 cells has been successfully used to simulate soft x-ray laser output with longer-laser-pulse (75 psec - 1 nsec) pumping. In our earlier work, it was found necessary to use a scale factor $F=0.5$ to multiply the actual incident-laser energy to account for unmodeled energy-loss channels in the absorption process [31]. In the present experiments, this value is no longer appropriate. As a result of extensive simulation we find that in all cases a lower value $F\sim 0.3$ gives better agreement (see, for example, Figs. 2 and 7). Since this empirical term is included to take into account a number of poorly enumerated factors, such as focus defects and plasma reflectivity, which vary from experimental system to system, it is not surprising that in these experiments, we find that a different factor gives an im-

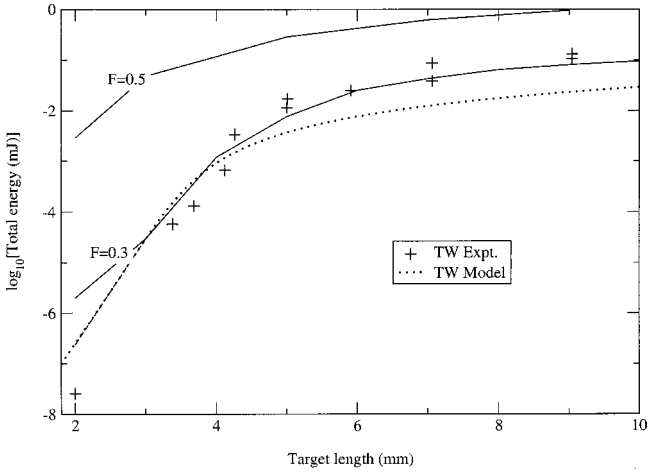

FIG. 7. Comparison of experimental output energies for the germanium laser in the traveling wave mode (TW) with those generated by direct simulation (full lines) and modeling. The analytic model (dotted) uses values taken from EHYBRID at 3.5 mm to calculate output energies for the TW system in the forward direction. Two values of the pump energy coupling factor F are shown for simulations with $F=0.3$ giving the best match.

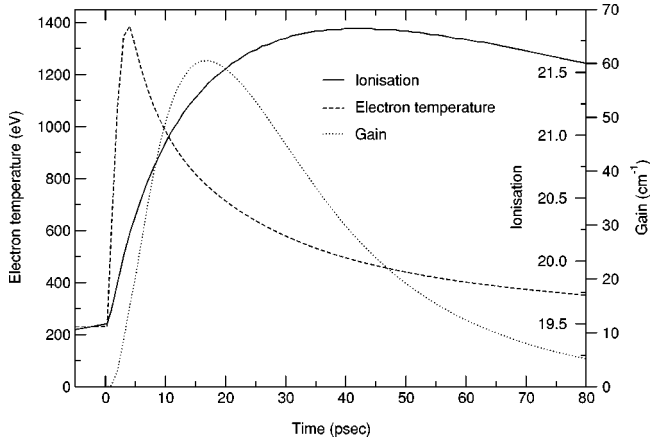

FIG. 8. Electron temperature, ionization, and peak gain of the 196 Å line at the location of peak gain as functions of time after main pulse onset, generated by EHYBRID modeling the experimental parameters given in the text.

proved fit to the experimental data obtained for the output scaling vs the pulse delay (Fig. 2) and the length (Fig. 7). On the other hand, if either or both are given the standard value 0.5, poor agreement is obtained. We also examined the output calculated when the absorption factor was set to $F=0.5$, and the monopole excitation rate reduced by 1/2 as in earlier work [31]. In this case the calculated output is too high at short lengths, when the laser is unsaturated, but closer to the measured values at long lengths. However, the overall agreement to experiments with these characteristics is markedly poorer than our new standard: $F=0.3$ and unmodified excitation rate.

A. Germanium Ne-like laser

Figure 2 shows the variation of the laser output from a 5 mm target for different time delays between the background and CPA pulses, compared with the values obtained by simulation. It can be seen that the best agreement is obtained when both pulses are assigned an absorption factor $F=0.3$. However, it can be seen that the simulation is much more sensitive to the value assigned to the long pulse. This result may be understood by examining the ionization history of the lasant under the optimum conditions (Fig. 8). It can be seen that prior to the CPA heating pulse, the ionization is only 19.5, and further ionization is required before peak gain is achieved. Increasing the F value of the long pulse increases the initial temperature and ionization and substantially increases the gain, as observed in Fig. 2. The sensitivity of the predicted output to the value of this parameter also probably explains the large shot-to-shot variation seen in many of the experimental results (Figs.2 and 3) in that relatively small shot-to-shot variations in the magnitude and spatial distribution of the focal spot, particularly from the background pulse, lead to marked differences in the overall output signal, especially before saturation is established. These effects are more marked in the NTW case, where saturation is weak, as observed experimentally.

As noted above, it is predicted that the ionization at the end of the long pulse is significantly less than the ideal in which the lasant is prepared in the closed-shell Ne-like configuration before the onset of strong heating. This result is consistent with experimental observations from the streaked x-ray spectrograph, which records the resonance spectra of the Ne- and F-like ionization stages. These lines are observed only after the commencement of the CPA pulse: a typical example of this behavior having been reported earlier [20]. In that case, the measured x-ray signal from these lines was shown to be in good agreement with the computational simulation.

1. Traveling wave operation

We now turn to a detailed consideration of the length scaling of the TW germanium laser. These simulations will refer only to the case discussed above, for which the temporal pulse structure has been optimized. Some aspects of this analysis have already been presented in an earlier paper [35] from which we draw a number of results.

Figure 7 shows the simulated output signal as a function of the length of the laser under the optimum condition with a delay of 50 psec for the CPA pulse. Agreement between simulation with $F\approx 0.3$ and the TW experimental results is good except at small gain lengths. The difference between simulation and experiment at short lengths (2 mm) can be accounted by late-time quasi-isotropic emission associated with recombination pumping of the upper-laser level [35], much of which lies outside the angular acceptance range of the detector. We may eliminate the contribution from these spurious signals, by truncating the output from RAYTRACE by following the natural decay of the signal. With this correction, the agreement is satisfactory.

The analytic model [35] can be used to create values of the output irradiance, from parameters generated with RAYTRACE data at peak output from a target of length 3.5

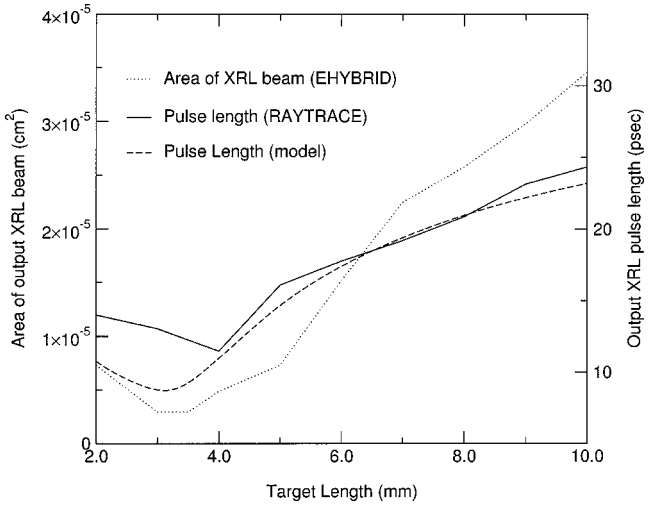

FIG. 9. Output pulse duration (full 1/e width) of the 196 Å line as a function of target length, as predicted by EHYBRID/RAYTRACE for the standard case (full line) and by the model (dotted). Also shown is the area of the output XRL beam as calculated by EHYBRID/RAYTRACE (dot dashed).

mm, i.e., just before the onset of saturation. The values of gain (50 cm^{-1}) and saturation irradiance (1.6×10^{10} W cm^{-2}) are in good agreement with the experimental estimates obtained earlier. However, the area and spontaneous emission rates vary depending on the target length considered. Figure 7 indicates that at short lengths the model closely matches both experiment and RAYTRACE values. However, the model seriously underestimates the output at long target lengths, where saturation is strong, by about a factor ~ 3.5 at length 9 mm. This is ascribed to the effect of saturation increasing the effective cross section of the lasing plasma (Fig. 9). This behavior, together with related pulse-length shortening and subsequent rebroadening, is due to the fact that once saturation sets in at the peak of the gain, rays still unsaturated make a proportionately greater contribution. These effects, associated with strong saturation, are accounted for by the temporal integration used for the RAYTRACE data. Calculation of the area (FWHM) of the near-field exit beam (Fig. 9) shows that increase in the effective area is $\sim 10\times$. Taking this into account, the model overestimates the output by a factor of $\sim 3\times$. This additional factor is ascribed both to the failure of some of the assumptions implicit in the model [36], in particular, the requirement of constant spontaneous emission irradiance, and also the uncertainty in the assignment of the exit area from the near-field pattern in RAYTRACE.

Pulse shortening is clearly seen in the simulation and analytic results (Fig. 9). However, the pulse shortening predicted by the model is greater than that obtained from the simulation. The resultant laser pulse is predicted to have a minimum value of the 1/*e* duration 11.5 psec from RAYTRACE at 4 mm and 10 psec at 3.25 mm from the model, as saturation sets in, compared to the gain lifetime of 35 psec. When the output is strongly saturated at 9 mm the laser-pulse length is increased to 24 psec. The simulation includes contributions from many rays, which have differing histories, and consequently, differing pulse shortening, which are averaged in the final signal. In contrast, the model considers only a single trajectory, albeit with ray-averaged parameters, and therefore exhibits the maximal shortening effect. A similar effect can also be seen in the area broadening noted above.

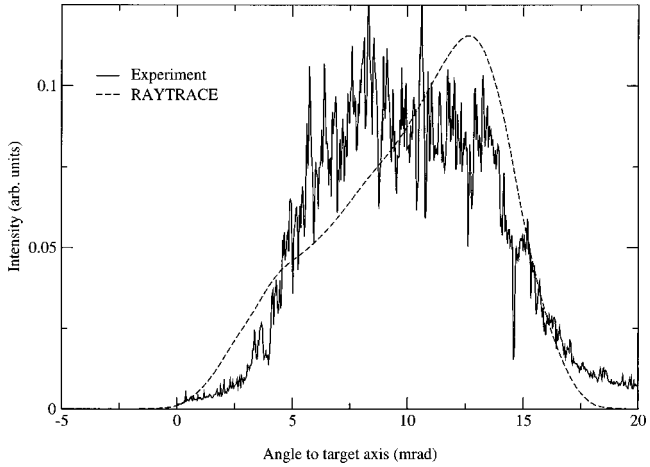

FIG. 10. Horizontal angular distributions for TW outputs from 9 mm targets of Ge obtained experimentally (solid) and by simulation (dotted).

The experiments also measured the beam far-field angular deflection and spread, which can be compared with simulation. With TW, the width and centroid of the beam are accurately predicted. The profiles differ slightly in form (Fig. 10), the simulation indicating slightly more rays traversing a longer path in the plasma, i.e., originating near the rear end of the laser. However, the results show that the density profile in the region of gain is modeled reasonably accurately.

2. Nontraveling wave operation

Figure 11 shows values of the output signal obtained from the NTW experiment, when the traveling wave was removed

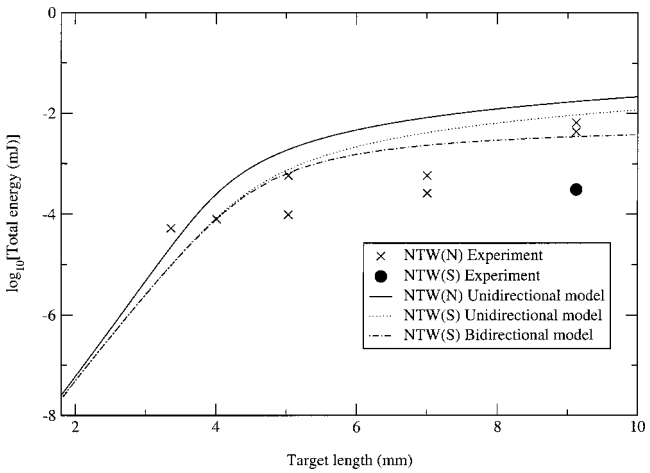

FIG. 11. Comparison of experimental output energies for the germanium laser at 196 Å in the nontraveling mode (NTW) with those modeled for the full gain pulse and group velocity equal to the velocity of light in vacuo. The models use values taken from EHYBRID at 3.5 mm to calculate output energies for the NTW systems in both the forward [NTW(N)] and backward [NTW(S)] directions.

and replaced by the natural progressive gain wave moving at 2.9*c* associated with the line-focusing optics. We have modeled this case using the gain temporal profile from EHYBRID, and ray-averaged parameters (spontaneous emission rate, gain, saturation irradiance, and beam area) obtained from the RAYTRACE, for a 1 psec CPA pulse duration and 3.5 mm target length, i.e., before saturation sets in. These results show that the lasing plasma has almost identical properties in both the TW and NTW cases despite the change in the CPA pulse duration. Since the output is now only weakly saturated at the longest lengths used, the strong saturation effects noted above are expected to be weak, and the model should give reasonable accuracy. For the forward (north) beam the unidirectional model is expected to be valid, but at lengths greater than about 7 mm the bidirectional should be used for the backward (south) beam. For the forward beam [NTW(N)] the unidirectional propagation model [20,35] shows reasonable agreement with the measured values at lengths up to 5 mm, but it overestimates the output by a factor of $\sim$2.5 at 9 mm. At these long lengths, the output has become weakly saturated, as may be seen by comparison with the TW results. The magnitude of this error is comparable to that found in the TW results, where an overestimate of $\sim$2.5 is found when the area effect is taken into account. In the NTW case, this (area) effect is negligible as may be seen by noting that at a target length of 9 mm, the NTW output is equal to that at 4 mm with TW. The corresponding area increase at this level of saturation is negligible (Fig. 9).

We have also modeled the limited experimental results (one data point) from the backward wave [NTW(S)]. In this case, it is necessary to include the effect of the saturation of the forward beam on the backward (bidirectional effects). The results are shown in Fig. 11 [NTW(S)] using the same values as above. Although the bidirectional calculation gives a marked improvement on that generated by the unidirectional model, the result still overestimates the experimental value by a factor $\sim$10, which may, in part, be due to the large shot-to-shot variation of the NTW x-ray laser output.

In earlier work, the knee in the NTW results at $\sim$3 mm was identified with the point at which the gain-pulse length became less that the transit time, i.e., the pulse duration was $0.3/c \sim 10$ psec. In fact, this interpretation is only valid if the pulse has a square profile. When the pulse has a smoothly varying form (as in Fig. 8), the pulse sharpening phenomenon discussed earlier plays a role, reducing the gain-pulse length. In order to explore this effect, we have modeled the NTW case using the EHYBRID generated values, and retained the same gain-pulse profile, but with a reduced $1/e$ width. In contrast to the TW case, the NTW output is very sensitive to variations of the gain-pulse lifetime from the value of 35 psec obtained from EHYBRID. As can be seen from Fig. 12, the NTW results are well accounted if the gain $1/e$ duration is reduced to 20 psec.

Despite these results, this short-pulse duration is not consistent with the experiments:

- If this hypothesis were correct, the angular profile of the NTW would be broader and closer to the axis than the TW: in fact, the opposite is the case (Fig. 6). The simulations show that the density profile is nearly stationary over the period of strongest gain. Since the gain lifetime (Fig. 9) is nearly equal to the transit time, the ray paths generating the output signal do not differ greatly between the TW and NTW cases. We note (Fig. 6) that the profiles are essentially the same, but that the deflection angle is less in the TW case, probably due to rays from lower density (hence, smaller deflection), which also give rise to the area increase noted earlier. On the other hand, the output generated by a short gain-life laser would consist of a continuous sequence of short pulses, uniformly generated along the laser; those from near the exit would suffer only small deflections. The NTW beam would in consequence be expected to be broad with a flat top starting near the axis.
- If the gain-pulse length were reduced, the output from the TW system would be reduced proportionately, thereby introducing a discrepancy with the experimental output of about a factor two into the RAYTRACE modeling at all lengths.

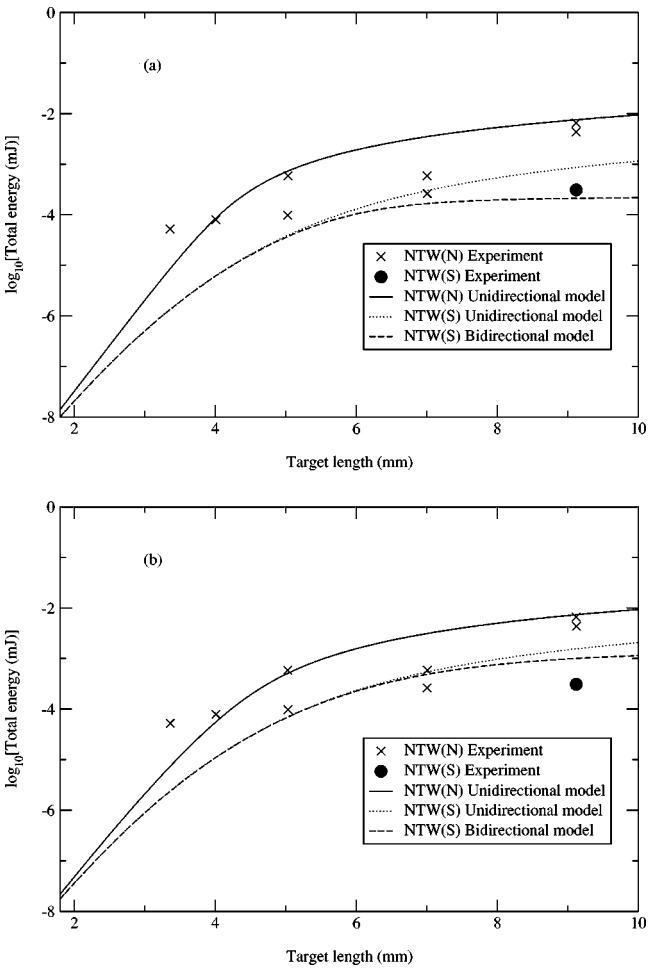

FIG. 12. Comparison of experimental output energies for the germanium laser at 196 Å in the nontraveling mode (NTW) with those modeled for a reduced gain pulse duration of 20 psec (a) and for reduced group velocity 0.5*c* (b). The models use values taken from EHYBRID at 3.5 mm to calculate output energies for the NTW systems in both the forward [NTW(*N*)] and backward [NTW(*S*)] directions.

Similar gain-pulse lengths were deduced by Nickles *et al.* [13] as a result of their experiments with Ti under similar conditions.

It has recently been proposed [37] that the observed saturation effects in short-pulse-pumped x-ray lasers can be explained by the reduction in the group velocity of the x-ray laser beam resulting from gain [38]. In order to explore this possibility, we have modeled the NTW data, which is more sensitive to timing mismatch, using the model with an adjustable group velocity for the x-ray laser beam. As can be seen from Fig. 12, a reduction of 0.5 from the velocity of light *in vacuo* is required to directly match the results, a value that implies a peak gain of 150 cm^{-1} [38]. From both the experimental and EHYBRID data, we find that the gain is 50 cm^{-1}, and the line width has a Doppler component 8.9×10^{11} Hz and Lorentz 4.9×10^{11} Hz. Adjusting the Casperson-Yariv result [39] for the corresponding Voigt profile, yields a group velocity $0.85c$, which is too large to have a significant effect.

An interesting observation can be made from Figs. 7 and 11 by comparing the gradients of the lines in the TW and NTW cases. The NTW output shows lower gain than TW, although the conditions are the same in each case. The strongest output in the TW case follows the peak gain along the axis, whereas that in the NTW is an average across the temporal profile of the gain due to the lack of synchronism between the pulses. Some evidence for this behavior can be seen in the experimental data (see Fig. 3).

B. Samarium Ni-like laser

We have used the same approach to model the samarium laser. However, in this case the active volume occupies a smaller space, and 400 cells were needed to give an accurate representation from EHYBRID. The other marked difference from the Ge is the shorter duration of the predicted output signal, which again demands a time resolution of at least 0.5 psec over the output to obtain accurate values. The samarium plasma has a gain profile with a relatively long lifetime ($\sim$22 psec). However, the laser output is dominated by a short duration ($\sim$4 psec) of high gain, which is superimposed on the long decay (Fig. 15). Analysis of the simulated ionization history again shows that the plasma is under ionized at the start of the CPA pulse. The short high-gain lifetime results from the rapidly cooled high-electron-temperature pulse generated by the pump. The slow overall gain decay results from the compensation of the declining excitation rate by an ionization increase.

Figure 4 compares the measured output signal at 9 mm target length with that obtained from the simulation as the pulse delay was varied. The optimum timing sequence is correctly predicted, together with the fall off at longer delay. However, when the CPA pulse is incident near the peak of the long pulse, the code gives negligible output in contrast to that found experimentally. Examination of the code output shows that at this time the ionization is incomplete and the plasma-density structure poorly developed. These two factors lead to low gain and enhanced refraction loss, with the result that the peak overall ray averaged gain-length product,

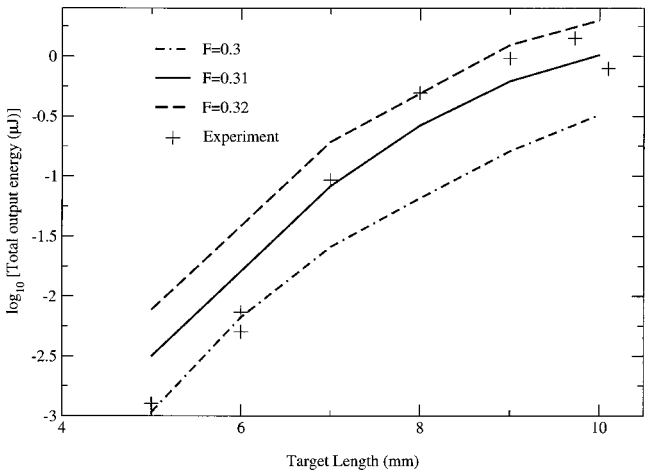

FIG. 13. Comparison of the output energy for the Ni-like Sm laser at 73 Å measured experimentally (points) with that obtained from simulation for different values of the absorption factor *F*.

when the CPA pulse is incident at the peak of the background pulse, is only $\lesssim1$, and hence, produces the weak output. A relatively small increase in the absorption *F* factor for the main pulse would increase the simulated x-ray laser output to the experimental value. Figure 13 shows the values of Ni-like Sm output at 73 Å generated by simulation compared with those found experimentally. It can be seen that relatively small changes in the absorption factor *F* produce significant changes in the output, the experimental values spanning the range of *F* modeled. At large gain-length (GL) products into saturation, the agreement is good. However, at low Gl, the same behavior is found as for germanium. Extrapolation of the signal at 6 mm. using the analytic model, with the EHYBRID-generated laser parameters at peak gain, again improves the modeling. At large Gl the analytic model underestimates both experimental and simulation outputs due to the increase in effective cross section resulting from saturation discussed earlier for germanium. The simulation results show that the duration ($1/e$ width) of the output pulse is 1.75 psec showing little variation with gain length.

The far-field beam profile in the radial direction is shown in Fig. 14. The simulation accurately calculates the angular beam width ($\sim$3 mrad), but underestimates the deflection by $\sim$1.5 mrad. However, as the experimental alignment accuracy of these short (10 mm) targets is probably not better than ±1 mrad (i.e., 10 μm in 10 mm), this error may be accounted for by experimental uncertainty. Otherwise, the origin of any discrepancy is poorly understood, but would probably result from an underestimate of the density gradient in the region of highest gain.

The characteristic gain profile noted earlier (Fig. 15) gives rise to very short-laser pulses of duration $\sim$1.7 psec. At large gain lengths, the output is dominated by the high-gain spike and the long-lived background makes only a small contribution to the signal, when the gain is less than $1/e$ of the peak value.

V. CONCLUSIONS

A traveling wave pump has been unequivocally demonstrated to achieve saturated operation of both Ne-like and

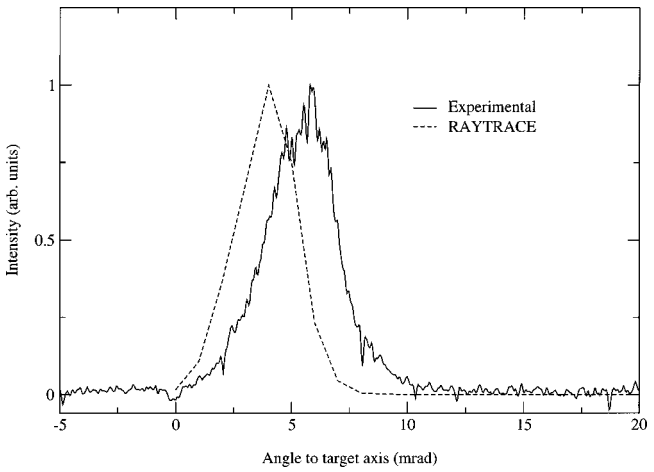

FIG. 14. Horizontal angular distributions for TW outputs from 9 mm targets of the Sm laser obtained experimentally (solid) and by simulation (dotted).

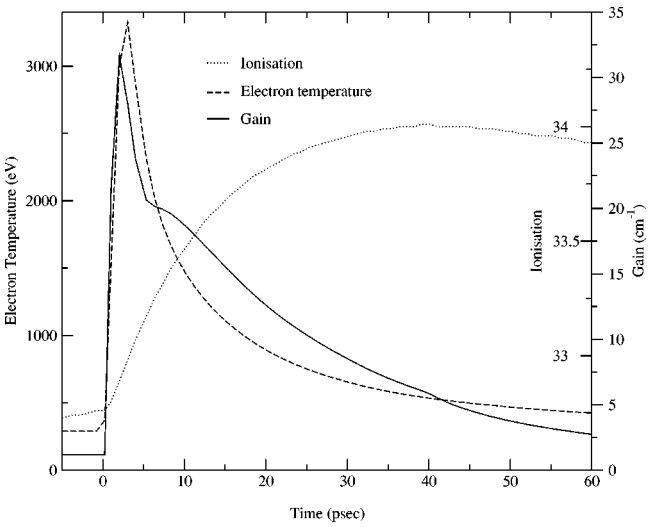

FIG. 15. Electron temperature, ionization and peak gain of the 73 Å line at the location of peak gain as functions of time after main pulse onset, generated by EHYBRID modeling the experimental parameters given in the text.

Ni-like x-ray lasers pumped with ~psec pulses. A high irradiance transient pump pulse, ~1 psec in duration, was focused into a preformed plasma column, ~10 mm in length, in such a way that the propagation speed of the plasma excitation region along the line column could be controlled and adjusted to match the speed of light. A gain coefficient of >40 cm^{-1} at 196 Å was produced in a Nelike Ge plasma, sufficient to saturate the $2p^5_{1/2}3p_{1/2}$ $J=0$ to $2p^5_{1/2}3s_{1/2}$ $J=1$ transition in a target $\geqslant 5$ mm long. Observations of both the forward and backward propagating x-ray laser beams under ideal and nonideal traveling-wave pump conditions have been made. Overall behavior has been shown to be consistent with numerical and semianalytical modeling. When Ni-like Sm targets were pumped under fully optimized traveling wave conditions, a small signal gain coefficient of ~19 cm^{-1} was observed at 73 Å on the $3d^9_{3/2}4d_{3/2}$ $J=0$ to $3d^9_{5/2}4p_{3/2}$ $J=1$ line and saturation effects were observed for targets $\geqslant 8$ mm long. This lasing is at approximately double the photon energy previously observed in ~psec pumping and is a direct consequence of a true TW pump.

The TW experiments at both 196 Å and 73 Å have been modeled in detail to determine their underlying behavior. Good agreement is found with the simulations using the codes for ionization/hydrodynamics EHYBRID and the beam propagation RAYTRACE. In these calculations we have used a modified atomic data set, which has enabled us to remove the empirical correction to the $J=0$-$J=0$ excitation rate introduced in earlier work to obtain good agreement with experiment. A second empirical factor E defined by the ratio of the energy absorpted in the plasma to the incident laser energy needs to be reduced from $F=0.5$ to $F=0.3$. These corrections have also been found to be applicable when comparing simulations to experiments with longer pulse durations and will be reported elsewhere.

The simulations, consistent with experiment, show that the initial state of ionization, before the CPA pulse starts, is less than ideal. In consequence, the optimal gain conditions are not achieved, and the effective gain lifetime ($1/e$ time) is longer than would otherwise be predicted. In the germanium case, the laser is strongly saturated, and the characteristic effects of saturation on traveling-wave behavior, modifying the pulse length and near-field beam area [35] are clearly demonstrated in the simulation. It was found that as a result, the minimum pulse length from the Ge laser at 196 Å is estimated to be about 13 psec., although the gain duration is about 35 psec. In contrast, the markedly different temporal gain profile of the Sm laser at 73 Å generates an output pulse just prior to saturation of only about 1.7 psec.

We have used semianalytical models to investigate the behavior of NTW lasers using the results obtained in these experiments. The fit between the predictions and measurements is not entirely satisfactory, but any conclusions drawn from this are limited by the inadequacies of the model and variability of the data. Two alternative hypotheses were investigated to see whether better agreement with experiment could be obtained. In the first, we reduced the effective gain duration to a value shorter than that consistently given by the TW simulations. In the second, we considered the effect of a reduced-group velocity on the laser radiation. In each case, by a suitable choice of appropriate parameters, the results could be adjusted to fit the experimental data. However, the modified values required were not consistent with those derived directly from the experiments or from the (more reliable) TW experiments.

ACKNOWLEDGMENTS

We acknowledge all the efforts of the VULCAN laser and target area staff. The work is grant supported in the United Kingdom by EPSRC and by the European Union TMR programme.

[1] J. Nilsen, B. J. MacGowan, L. B. DaSilva, and J. C. Moreno, Phys. Rev. A **48**, 4682 (1993).

[2] J. Nilsen and J. C. Moreno, Phys. Rev. Lett. **74**, 337 (1995); Opt. Lett. **20**, 1386 (1995).

[3] H. Daido, Y. Kato, K. Murai, S. Ninpmiya, R. Kodama, G. Yuan, Y. Oshikane, M. Takagi, and H. Takabe, Phys. Rev. Lett. **75**, 1074 (1995).

[4] P. J. Warwick, C. L. S. Lewis, S. McCabe, A. G. Macphee, A. Behjat, M. Kurkcuoglu, G. J. Tallents, D. Neely, E. Wolfrum, S. B. Healy, and G. J. Pert, Opt. Commun. **144**, 192 (1997); A. G. MacPhee, C. L. S. Lewis. P. J. Warwick, I. Weaver, A. Carillon, G. Jamelot, A. Klisnick, B. Rus, P. Zeitoun, M. Nantel, P. Goedkindt, S. Sebban, G. J. Tallents, A. Demir, M. Holden, and J. Krishnan, *ibid.* **133**, 525 (1997).

[5] J. A. Plowes, G. J. Pert, and P. B. Holden, Opt. Commun. **116**, 260 (1995); **117**, 189 (1995); J. A. Plowes, G. J. Pert, S. B. Healy, and D. T. Toft, Opt. Commun. **28**, 219 (1996).

[6] Y. Li, G. Pretzler, E. E. Fill, and J. Nilsen, J. Opt. Soc. Am. B **13**, 742 (1996); A. Sureau and P. B. Holden, Phys. Rev. A **52**, 3110 (1995); S. Jacquemot and L. Bonnet, Proc. SPIE **2012**, 180 (1993).

[7] J. Zhang, A. G. MacPhee, J. Nilsen, J. Lin, T. W. Barbee, Jr., C. Danson, M. H. Key, C. L. S. Lewis, D. Neely, R. M. N. O'Rourke, G. J. Pert, R. Smith, G. J. Tallents, J. S. Wark, and E. Wolfrum, Phys. Rev. Lett. **78**, 3856 (1997); J. Zhang, A. G. MacPhee, J. Lin, E. Wolfrum, R. Smith, C. Danson, M. H. Key, C. L. S. Lewis, D. Neely, J. Nilsen, G. J. Pert, G. J. Tallents, and J. S. Wark, Science **276**, 1097 (1997).

[8] R. Smith, G. J. Tallents, J. Zhang, G. Eker, S. McCabe, G. J. Pert, and E. Wolfrum, Phys. Rev. A **59**, R47 (1999).

[9] J. Y. Lin, G. J. Tallents, R. Smith, A. G. MacPhee, E. Wolfrum, J. Zhang, G. Eker, R. Keenan, C. L. S. Lewis, D. Neely, R. M. N. O'Rourke, G. J. Pert, S. J. Pestehe, and J. S. Wark, J. Appl. Phys. **85**, 672 (1998).

[10] M. Tagviashvili and G. J. Tallents, in *X-ray Lasers 1998*, edited by Y. Kato and H. Daido, Institute of Physics (IOP) Conference Series No. 159 (IOP, Bristol, 1999), p. 439.

[11] P. A. Simms, S. McCabe, and G. J. Pert, Opt. Commun. **153**, 164 (1998).

[12] S. McCabe and G. J. Pert, Phys. Rev. A **61**, 033804 (2000).

[13] P. V. Nickles, V. N. Shlyaptsev, M. P. Kalachnikov, M. Schnürer, I. Will, and W. Sandner, Phys. Rev. Lett. **78**, 2748 (1997); M. P. Kalachnikov, P. V. Nickles, M. Schnürer, W. Sandner, V. N. Shlyaptsev, C. Danson, D. Neely, E. Wolfrum, J. Zhang, A. Behjat, A. Demir, G. J. Tallents, P. J. Warwick, and C. L. S. Lewis, Phys. Rev. A **57**, 4778 (1998).

[14] G. J. Tallents, J. Y. Lin, J. Zhang, A. Behjat, A. Demir, M. M. Güzelgöz, C. L. S. Lewis, A. G. MacPhee, D. Neely, G. J. Pert, R. Smith, J. S. Wark, P. J. Warwick, and E. Wolfrum, OSA Tech. Digest Series **7**, 47 (1997).

[15] J. Dunn, A. L. Osterheld, R. Shepherd, W. E. White, V. N. Shalyaptsev, and R. E. Stewart, Phys. Rev. Lett. **80**, 2825 (1998).

[16] A. Klisnick, D. Ros, P. Zeitoun, F. Albert, A. Carillon, P. Foucade, S. Hubert, P. Jaeglé, G. Jamelot, C. L. S. Lewis, A. MacPhee, R. O'Rourke, R. Keenan, P. Nickles, K. Janulewicz, M. Kalashnikov, J. Warwick, J. C. Canteloup, E. Salmon, C. Sauteret, J. P. Zou, D. Joyeux, and D. Phalippou, in *X-ray Lasers 1998*, Institute of Physics (IOP) Conference Series No. 159, edited by Y. Kato and H. Daido (IOP, Bristol, 1999), p. 107.

[17] A. Klisnick, P. Zeitoun, D. Ros, A. Carillon, P. Foucade, S. Hubert, G. Jamelot, C. L. S. Lewis, A. MacPhee, R. O'Rourke, R. Keenan, P. Nickles, K. Janulewicz, M. Kalashnikov, J. Warwick, J. C. Canteloup, A. Migus, E. Salmon, C. Sauteret, and J. P. Zou, J. Opt. Soc. Am. B **17**, 1093 (2000)

[18] Yu. V. Afanasiev and V. N. Shlyaptsev, Kvant. Elektron. (Moscow) **16**, 2499 (1989) [Sov. J. Quantum Electron. **19**, 1606 (1989)]; V. N. Shylaptsev, P. N. Nickles, T. Schlegel, M. P. Kalashnikov, and A. L. Osterheld, Proc. SPIE **2012**, 111 (1993).

[19] S. B. Healy, K. A. Janulewicz, J. A. Plowes, and G. J. Pert, Opt. Commun. **132**, 442 (1996); J. Nilsen, Phys. Rev. A **55**, 3271 (1997).

[20] J. Y. Lin, G. J. Tallents, A. G. MacPhee, A. Demir, C. L. S. Lewis, R. M. N. O'Rourke, G. J. Pert, D. Ros, and P. Zeitoun, Opt. Commun. **166**, 211 (1999).

[21] J. Dunn, Y. Li, A. L. Osterheld, J. Nilsen, J. R. Hunter, and V. N. Shlyaptsev, Phys. Rev. Lett. **84**, 4834 (2000).

[22] C. N. Danson, P. V. Nickles, R. Allott, A. Behjat, J. Collier, A. Demir, M. P. Kalachnikov, M. H. Key, C. L. S. Lewis, D. Neely, D. A. Pepler, G. J. Pert, M. Schnürer, W. Sandner, V. P. Shlyaptsev, G. J. Tallents, P. J. Warwick, E. Wolfrum, and J. Zhang, AIP Conf. Proc. **426**, 473 (1998).

[23] C. P. J. Barty, D. A. King, G. Y. Yin, K. H. Hahn, J. E. Field, J. F. Young, and S. E. Harris, Phys. Rev. Lett. **61**, 2201 (1988).

[24] L. B. Da Silva, B. Cauble, G. Frieders, J. A. Koch, B. MacGowan, D. L. Matthews, S. Mrowka, D. Ress, J. E. Trebes, and T. Weiland, Proc. SPIE **2012**, 158 (1993).

[25] J. L. Collier, D. Pepler, C. Danson, J. Warwick, C. Lewis, and D. Neely, in *Central Laser Facility Rutherford Appleton Laboratory Annual Report*, RAL Report **TR-97-045**, 209 (1998); J. L. Collier, C. N. Danson, R. M. Allott, M. H. R. Hutchinson, C. L. S. Lewis, D. Neely, D. A Pepler, T. B. Winstone, and J. Zhang, in *X-ray Lasers 1998*, edited by Y. Kato and H. Daido, Institute of Physics (IOP) Conference Series No. 159 (IOP, Bristol, 1999), p. 649.

[26] J-C. Chanteloupe, E. Salmon, J. P. Zou, A. Migus, C. Sauteret, P. Zeitoun, A. Klisnick, A. Carrilon, S. Hubert, D. Ros, C. L. S. Lewis, A. MacPhee, R. O'Rourke, R. Keenan, P. Nickles, K. Janulewicz, M. Kalashnikov, and J. Warwick, in *X-ray Lasers 1998*, Institute of Physics (IOP) Conference Series No. 159, edited by Y. Kato and H. Daido (IOP, Bristol, 1999), p. 653.

[27] Andor Technology Ltd, 9 Millennium Way, Springvale Business Park, Belfast T12 7AL, Northern Ireland.

[28] F. Strati, G. J. Tallents, G. J. Pert, C. L. S. Lewis, R. Keenan, S. Topping, A. Klisnick, D. Ros, J. Kuba, R. Smith, A. G. MacPhee, D. Neely, R. Allot, R. Clarke, P. Bartolotti, P. Nickles, and K. Janulewicz, Central Laser Facility Ann. Rept. [ISBN 0902376012] **RAL-TR-2000-034**, 52 (2000).

[29] G. J. Linford, E. R. Peressini, W. R. Sooy, and M. L. Spaeth, Appl. Opt. **13**, 379 (1974).

[30] L. B. Da Silva, B. J. MacGowan, R. A. London, J. A. Koch, S. Mrowka, D. L. Matthews, and J. H. Underwood, Opt. Lett. **18**, 1174 (1993).

[31] P. B. Holden, S. B. Healy, M. T. M. Lightbody, G. J. Pert, J. A. Plowes, A. E. Kingston, E. Robertson, C. L. S. Lewis, and D. Neely, J. Phys. B **27**, 341 (1994); S. B. Healy, G. F. Cairns, C.

L. S. Lewis, G. J. Pert, and J. A. Plowes, IEEE J. Sel. Top. Quantum Electron. **1**, 940 (1995); G. F. Cairns, S. B. Healy, C. L. S. Lewis, G. J. Pert, and E. Robertson, J. Phys. B **29**, 4839 (1996).

[32] K. G. Dyall, I. P. Grant, C. T. Johnson, F. A. Parpia, and E. P. Plummer, Comput. Phys. Commun. **55**, 425 (1989).

[33] H. L. Zhang, D. H. Sampson, and C. J. Fontes, At. Data Nucl. Data Tables **48**, 91 (1991).

[34] P. J. Warwick and C. L. S. Lewis, Central Laser Facility Ann. Rept. **RAL-TR-97-045** [ISBN 0902376705], 99 (1998); F. Strati and G. J. Tallents, Central Laser Facility Ann. Rept. **RAL-TR-99-062** [ISBN 0902376950], 73 (1999); F. Strati and G. J. Tallents, Proceedings of the Seventh Conference on X-ray Lasers (St. Malo) (to be published).

[35] R. E. King and G. J. Pert, Compte Rendus Serie IV **1**, 1093 (2000).

[36] G. J. Pert, Optics Commun. **191**, 113 (2001)

[37] R. Tommasini and E. Fill, Phys. Rev. A **62**, 034701 (2000).

[38] F. Strati and G. J. Tallents, Phys. Rev. A **64**, 013807 (2001).

[39] L. Casperson and A. Yariv, Phys. Rev. Lett. **26**, 293 (1971).